

A novel geometric phase for optical beams

Kristina Frizyuk^{*1}, Evgenii Menshikov², and Mauro Spera³

¹Institute of Theoretical Solid State Physics, Karlsruhe Institute of Technology, Karlsruhe, Germany

²Department of Information Engineering, University of Brescia, Brescia, Italy

³Dipartimento di Matematica e Fisica “Niccolò Tartaglia”, Università Cattolica del Sacro Cuore, Brescia, Italy

Abstract

In this paper, we provide an accurate description of geometric phases emerging in simple optical systems — nanostructures (metaatoms) interacting with vortex beams. We show that this interaction leads to a new class of geometric phase for optical beams, which is different from the geometric phases commonly discussed in structured-light optics. We compare this setting to the usual description of geometric phases for beams and show that the underlying geometry is different.

Keywords: Pancharatnam-Berry phase, vortex beams, nanostructures, holonomy.

Contents

1	Introduction	2
2	The simplest case of the Pancharatnam phase	2
2.0.1	Poincaré and Riemann sphere	3
2.1	Differential geometric viewpoint	5
2.1.1	Fibre bundles	6
2.1.2	Connections	6
2.1.3	Geometry of the Hopf bundle	7
2.1.4	Horizontal lift and holonomy	9
2.1.5	Action of the waveplate	9
3	Vortex beams. Main result.	10
3.1	Vortex beams via the Hermite-Gaussian sphere	12
3.2	Majorana representation	14
4	Discussion	14
5	Conclusions	15
6	Acknowledgements	16
A	Stereographic Projection	16

^{*}Email: kristina.friziuk@kit.edu

B Projective space	17
C Derivations for the $SU(2)$ matrix for the rotated waveplate	17
C.1 Horizontal lift and holonomy: an example	18
C.2 Global and local descriptions	19
C.3 Curvature and Chern classes	20
D $SU(2)$-actions and parallel transport	21
E Interpretation in terms of coherent states	22
F Details of numerical simulations	23

1 Introduction

Geometric phases are widely used in optics [1, 2] for different applications. The simplest one is transmission of polarized plane wave through a waveplate [3, 4], corresponding to the rotation of Poincaré sphere around a horizontal axis. One of the most well-known are Pancharatnam-Berry metasurfaces, mostly based on similar birefringence-like effect of single metaatoms [5–13]. Geometric phases can be also introduced for beams with angular momentum [1, 14–18]. The following question then arises: why are these particular type of phases called “geometric”? What is then the underlying geometry? This question has been initially addressed in [19], which connects the phase, introduced by Berry with the holonomy of a connection on a line bundle. Here, we discuss the geometric phases for vortex beams from this point of view, via an explicit description of the underlying topological and geometrical objects, also providing a new type of geometric phase for beams, which was apparently never discussed previously. The effect enables mode-selective phase control and discrimination of vortex beams based on their total angular momentum, using simple nanostructures, offering a practical alternative to spatial light modulators and multi-element polarization schemes.

We first start with the description of the simplest well-known case of a waveplate and circularly polarized plane waves, and later generalize it by introducing a new type of geometric phase for optical beams. Then we provide a mathematical description of the well-known geometric phase for beams, showing the emergence of a different geometry.

The paper is organized as follows: in Section 2 we revisit the well-known Pancharatnam geometric phase and describe its geometry in detail. In Section 3 we theoretically describe a novel type of geometric phase for vortex beams, whose geometry different from the known ones, and compare the ensuing geometric descriptions. In Section 4, we discuss the terminology and geometric interpretation of optical phases, and outline open conceptual issues concerning geometric phases in linear and nonlinear optics.

2 The simplest case of the Pancharatnam phase

In this section, we describe the case of a polarized wave passing through a waveplate in some detail [20–22].

2.0.1 Poincaré and Riemann sphere

The polarization state of light \mathbf{E} in the basis of right $|R\rangle$ and left-polarized $|L\rangle$ plane waves can be described by two complex numbers $(E_R, E_L) \in \mathbb{C}^2$:

$$\mathbf{E} = E_R |R\rangle + E_L |L\rangle = E_x |B_e\rangle + E_y |B_o\rangle \quad (1)$$

where

$$|B_e\rangle = \frac{|R\rangle + |L\rangle}{\sqrt{2}}, \quad |B_o\rangle = -i \frac{|R\rangle - |L\rangle}{\sqrt{2}}, \quad (2)$$

and E_R and E_L are complex numbers that fully encode the field state. However, for determining polarization states, only the relative amplitude and phase matter; the overall amplitude and any global phase factor are irrelevant. Let us introduce the vector:

$$\Psi = \begin{pmatrix} E_R \\ E_L \end{pmatrix}, \quad (3)$$

which is analogous to the Jones vector for linear polarization. Since the overall amplitude and phase of Ψ do not affect the polarization state, we can normalize this vector and consider only the ratio of E_R to E_L , represented as a complex number $z = E_R/E_L$. The complex plane may be compactified to a Riemann sphere, with homogeneous coordinates $[E_R : E_L]$ (see Appendix B). The Poincaré sphere then provides a way of parametrizing polarization states in a unique fashion. The mapping from the complex plane to the Poincaré sphere is given by the stereographic projection (see Appendix A and [23]):

$$z = \cot\left(\frac{\theta}{2}\right) e^{i\varphi}, \quad (4)$$

where θ is the polar angle from the north pole of the Poincaré sphere and φ is the azimuthal angle. This equation shows how a point on the complex plane is related to a point on the Poincaré sphere, with θ and φ describing the polarization state. The north and south poles of the Poincaré sphere ($\theta = 0$ and $\theta = \pi$, respectively) correspond to right and left circular polarizations, while points on the equator ($\theta = \pi/2$) represent linear polarizations (see Fig. 1a). The remaining points represent elliptical polarizations, with the azimuthal angle φ indicating the orientation of the ellipse.

Let us consider the action of a waveplate on an arbitrarily polarized plane wave (1). Note that the same consideration is applicable to the case depicted in Fig. 1b, where the nanostructure with C_{2v} or D_{2h} symmetry plays the role of a conventional waveplate made from a uniaxial crystal. This happens partly because the eigenmodes along x - and y - are non-degenerate and excited with different phases, depending on their resonant frequencies [24, 25]. First we consider the case when the waveplate is oriented with optical axis along the x -direction. As such, it just provides an additional phase δ between the components of the input Jones vector $\mathbf{E} = (E_x, E_y)^\top$. For convenience, we write the new vector as $\tilde{\mathbf{E}} = (E_x e^{i\delta/2}, E_y e^{-i\delta/2})^\top$. Using

$$E_R = \frac{E_x - iE_y}{\sqrt{2}}, \quad E_L = \frac{E_x + iE_y}{\sqrt{2}}, \quad (5)$$

$$E_x = \frac{E_R + E_L}{\sqrt{2}}, \quad E_y = -\frac{E_R - E_L}{i\sqrt{2}}. \quad (6)$$

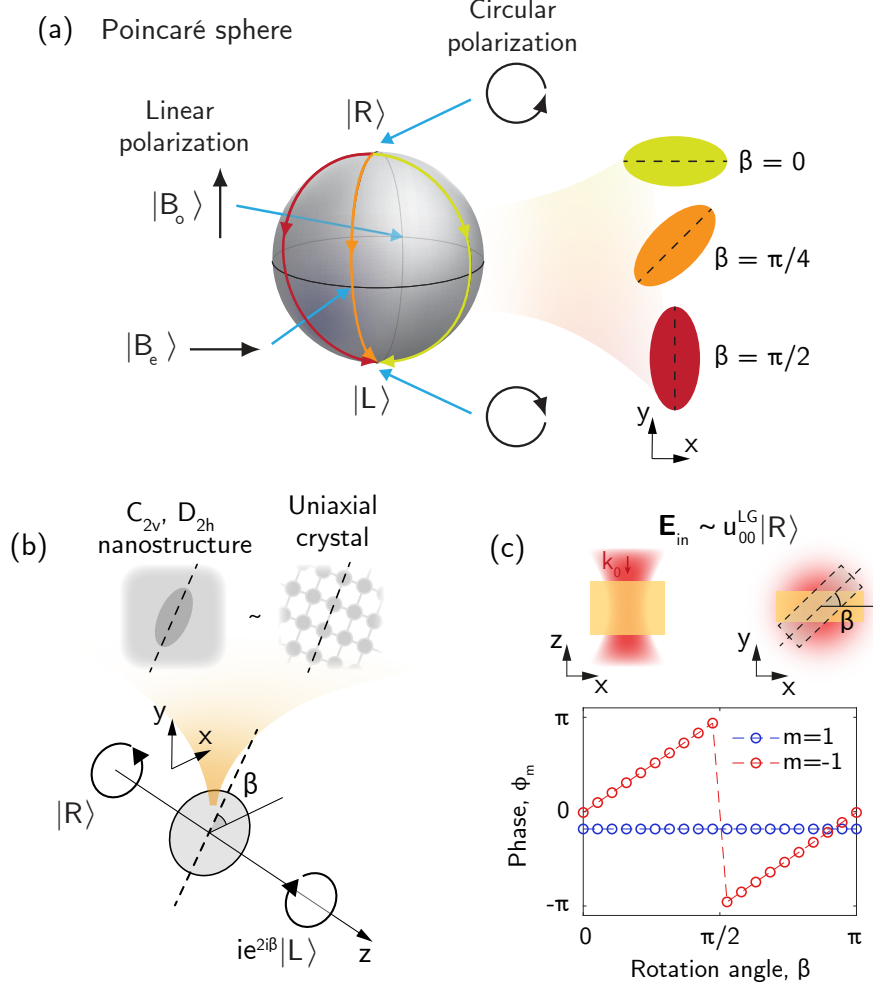


Figure 1: Poincaré sphere and examples of nanostructures for a geometric-phase experiment. (a) Depending on the rotation β of the structure, the Poincaré sphere rotates around different axes. The path corresponds to the case where incident RCP light is converted to LCP light upon transmission through such a structure. (b) Schematic of the setup illustrating geometric phase. (c) Numerically calculated phase acquired upon rotation of a rectangular nanoparticle under excitation by a fundamental Gaussian beam.

we obtain new values \tilde{E}_L and \tilde{E}_R after the waveplate:

$$\begin{pmatrix} \tilde{E}_L \\ \tilde{E}_R \end{pmatrix} = \begin{pmatrix} \cos \delta/2 & i \sin \delta/2 \\ i \sin \delta/2 & \cos \delta/2 \end{pmatrix} \begin{pmatrix} E_L \\ E_R \end{pmatrix} = (\mathbb{I} \cos \delta/2 + i \sigma_x \sin \delta/2) \begin{pmatrix} E_L \\ E_R \end{pmatrix}. \quad (7)$$

Here σ_x is one of Pauli matrices

$$\sigma_x = \begin{pmatrix} 0 & 1 \\ 1 & 0 \end{pmatrix}, \quad \sigma_y = \begin{pmatrix} 0 & -i \\ i & 0 \end{pmatrix}, \quad \sigma_z = \begin{pmatrix} 1 & 0 \\ 0 & -1 \end{pmatrix}. \quad (8)$$

If the phase shift corresponds to half-wave retardation, $\delta = \pi$, we have $E_L \rightarrow iE_R$, $E_R \rightarrow iE_L$. Let us check what happens if we rotate the optical axis of the waveplate, so as to form a β degrees angle with the x -axis. We provide the derivations for this case in Appendix C. Eventually, we get the general formula for an arbitrary waveplate (or a nanostructure with

2-fold rotational symmetry):

$$\begin{pmatrix} \tilde{E}_L \\ \tilde{E}_R \end{pmatrix} = (\mathbb{I} \cos \delta/2 + i(\cos 2\beta \sigma_x + \sin 2\beta \sigma_y) \sin \delta/2) \begin{pmatrix} E_L \\ E_R \end{pmatrix}. \quad (9)$$

Importantly, we see that this transformation is performed via $SU(2)$ matrix. One can indeed easily check that determinant of this matrix is equal to 1, and $U^\dagger U = 1$. Finally, for $\beta = 45^\circ$ we get

$$\begin{pmatrix} \tilde{E}_L \\ \tilde{E}_R \end{pmatrix} = (\mathbb{I} \cos \delta/2 + i\sigma_y \sin \delta/2) \begin{pmatrix} E_L \\ E_R \end{pmatrix}. \quad (10)$$

In this case for $\delta = \pi$ we have $E_L \rightarrow E_R$, $E_R \rightarrow -E_L$. And generally, for $\delta = \pi$ we get

$$\begin{pmatrix} \tilde{E}_L \\ \tilde{E}_R \end{pmatrix} = \begin{pmatrix} 0 & ie^{-2i\beta} \\ ie^{2i\beta} & 0 \end{pmatrix} \begin{pmatrix} E_L \\ E_R \end{pmatrix} \quad (11)$$

We cannot realize a rotation around the z -axis by a waveplate, but we can do this via some kind of gyroscopic medium [4, 26, 27]. The group $SU(2)$ is a double covering (indeed, the universal covering group) of the group $SO(3)$ consisting of all (special, *i.e.* with unit determinant) rotations of the Poincaré sphere [21, 28–30]. This means that actually two $SU(2)$ matrices correspond to each rotation of the Poincaré sphere. One can check that during any transformation of the form (9), all points of the Poincaré sphere are just rotated around some horizontal axis. For this, one should keep in mind the relation between Stokes parameters and Jones matrices [31, 32] and compare with Chapter IV.5 “ $SU(2)$: Double Covering and the Spinor” in [28]. For convenience, we restrict our attention to the evolution of an initially circularly polarized state. The path of this state is drawn in Fig. 1a. Depending on the thickness of the wave-plate, the path may have different lengths, so the a path is parametrized by thickness. Using (11) it is easy to see that the final phases will be different, and β - dependent. For two different paths which that cut out a slice (a closed contour) from the sphere, the phase difference will be equal to the half of the solid angle $\Omega/2$ [2].

Figure 1c shows the numerically calculated geometric phase acquired by a rectangular nanoparticle in air (D_{2h}) under illumination by a right circularly polarized (RCP) fundamental Gaussian beam ($l = p = 0$, see also Sec. F). In this case for the cross polarized projection (LCP, $m = -1$), the phase follows the $e^{2i\beta}$ law, and a full trip around the equator of the Poincaré sphere is completed when the the particle is rotated by an angle $\beta = \pi$, while the phase of the co-polarized component ($m = 1$) does not depend on β .

2.1 Differential geometric viewpoint

Let us now consider the simple experiment discussed above from a differential geometric point of view. For the basic definitions, one may also consult [33–35]. In general, when the polarization state on the Poincaré sphere (S^2) traverses a closed path, the actual state of light (including the common phase) traces a path in another, higher-dimensional space (see Fig. 2) which, in our specific case, is given by the three-dimensional sphere S^3 . In this space, the path is not necessarily closed; its behavior is in fact determined by the specific way in which the point moves, physically via a waveplate and mathematically through the *holonomy* of a connection [35–37] — measuring the extent to which the path fails to close — which actually represents the geometric phase.

The three-dimensional sphere is fibred into circles (corresponding to the total phase), each of which is projected onto a single point on S^2 . This construction corresponds to the so-called Hopf fibration. Some intuition can be gained from specifically dedicated videos, see e.g. [23, 38].

2.1.1 Fibre bundles

When we forget the total phase, and consider only the polarization, we have a point on a Poincaré sphere. This sphere will be called a base space. The total phase (we could deal with the amplitude as well, but we shall not do this here) can be depicted as a point on a circle S^1 . Thus, to each point on the Poincaré sphere there corresponds a circle, accommodating the total phase. So we can imagine the circles “attached” to the sphere as the teeth of a comb are attached to its base. The whole system is a **fibre bundle**, with a total space E , base space $B = S^2$ and fiber $F = S^1$ (see Fig. 2) [34, 35]. We denote this arrangement as (E, B, π, F) . Here $\pi: E \rightarrow B$ is projection which maps each fiber F_x , $x \in B$, to the point x itself. We will discuss the structure of the total space E in our case in detail later on.

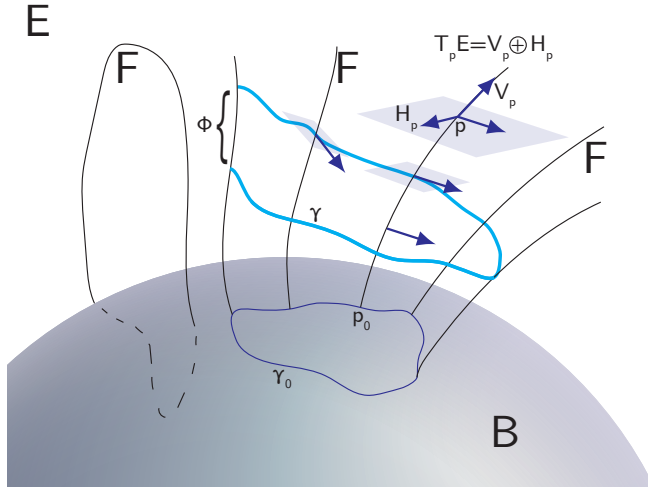


Figure 2: Illustration of the circle bundle over the sphere S^2 . Fibers F are topologically circles S^1 , the base manifold is a sphere S^2 . The horizontal lift γ of the curve γ_0 via a connection is shown. The tangent space to the total space E at a point $p \in E$, $T_p E$ is shown, together with its decomposition as the direct sum of a horizontal and vertical subspace. Horizontal subspaces are determined by a connection form. The holonomy ϕ of the connection is the geometric phase.

We will work with locally trivial fibre bundles, i.e., those obtained by appropriately “gluing” trivial bundles (E, U, π, F) with $E = U \times F$, where $U \subseteq B$ is an open set from an open cover of B and $\pi: E \rightarrow U$ is the projection onto U ; that is, for $(x, f) \in U \times F$, $\pi(x, f) = x$. The detailed construction of a locally trivial fibre bundle is not essential for our purposes; it suffices to know that our bundle is “good enough”.

2.1.2 Connections

However, since there is no canonical way to identify the fibres with each other, we need an additional structure, a *connection*, that specifies how neighbouring fibres are “glued together”. For this purpose, we introduce horizontal and vertical subspaces of the tangent space $T_p E$ to some point p of the total space E .

The **vertical subspace** V_p is the subspace of the tangent space $T_p E$ that consists of vectors that are tangent to the fibers. Formally, it is defined as:

$$V_p = \{u \in T_p E \mid \pi_* u = 0\}, \quad (12)$$

where $\pi: E \rightarrow B$ is the projection map, and $\pi_* u$ denotes the pushforward of u , recalled below.

Pushforward: Let $f: M \rightarrow N$ be a smooth map between manifolds M and N . The pushforward of f , denoted f_* , is a map between the tangent spaces $T_p M$ and $T_{f(p)} N$ that sends a vector $v \in T_p M$ to a vector $f_* v \in T_{f(p)} N$. Informally, if some vector v was a tangent vector to a particular curve, after a pushforward, it becomes a tangent vector of the image of this curve after the action of the function f .

$$f_*: T_p M \rightarrow T_{f(p)} N \quad (13)$$

The **horizontal subspace** H_p at a point p in the bundle E is a subspace of the tangent space $T_p E$ that complements the vertical space. The term ‘‘horizontal’’ should not be understood as implying orthogonality to the vertical subspace, as no metric has been introduced so far. A **connection** on a bundle (E, B, π, F) can be described in terms of a connection form \mathcal{A} . The **connection form** \mathcal{A} is a 1-form on E with values in the vertical subspace. Its action on a tangent vector $u \in T_p E$ is given by:

$$\mathcal{A}_p(u) := \text{ver } u \in V_p, \quad (14)$$

where $\text{ver } u$ denotes the vertical component of u . Concretely, this 1-form just takes a vector from the tangent space $T_p E$ and returns its projection onto the vertical subspace V_p , namely the component tangent to the fiber. Equivalently, a connection specifies a complement H_p to the vertical subspace V_p and picks up the vertical component of a vector in $T_p E$: in other words, it is the (oblique) projection onto V_p along H_p . Explicitly, the **horizontal subspace** is defined as follows:

$$H_p = \{u \in T_p E \mid \mathcal{A}_p(u) = 0\}.$$

Vertical and horizontal components are depicted in Fig. 2. The definitions above were quite general, but for the physical problems under consideration here, we are basically interested in the celebrated Hopf bundle, to be discussed below.

2.1.3 Geometry of the Hopf bundle

We shall illustrate the above general scheme in the important specific case provided by the Hopf bundle, shortly \mathcal{H} , following [34]. The total space in this case is a three-dimensional sphere S^3 , embedded in the four-dimensional space \mathbb{C}^2 , as

$$|z_1|^2 + |z_2|^2 = 1. \quad (15)$$

The base space is the two-dimensional sphere S^2 . The projection map $\pi: S^3 \rightarrow S^2$ reads

$$\pi(z_1, z_2) = (2 \operatorname{Re}(z_1 \overline{z_2}), 2 \operatorname{Im}(z_1 \overline{z_2}), |z_1|^2 - |z_2|^2) = (x, y, z). \quad (16)$$

These expressions for the three components resemble the Stokes parameters (with a change in notation), and this is not a coincidence. One can check that, actually, $x^2 + y^2 + z^2 = 1$. Note that

$$\pi(z_1, z_2) = \pi(e^{i\alpha} z_1, e^{i\alpha} z_2), \quad (17)$$

The fibre F is the circle $S^1 \approx U(1)$ (that is, we have a *principal bundle* with *structure group* $G = U(1)$) and the above formula says that the projection is invariant under the action of $U(1)$ group.

Let us now define a “canonical” connection. Let $\langle \cdot, \cdot \rangle: \mathbb{C}^2 \rightarrow \mathbb{C}$ be the standard Hermitian inner product in \mathbb{C}^2 . For any $(z_1, z_2), (w_1, w_2) \in \mathbb{C}^2$, it is defined as:

$$\langle (z_1, z_2), (w_1, w_2) \rangle := \bar{z}_1 w_1 + \bar{z}_2 w_2. \quad (18)$$

Let us consider a point $p \in S^3$ and take any vector $v \in T_p S^3$. If $p \in S^3$ corresponds to $(z_1, z_2) \in \mathbb{C}^2$, then the vertical space V_p is defined as

$$V_p = \{(\alpha z_1, \alpha z_2) \mid \alpha \in \mathbb{C}\}. \quad (19)$$

For the horizontal space, we take

$$H_p = \{(w_1, w_2) \in \mathbb{C}^2 \mid \langle (z_1, z_2), (w_1, w_2) \rangle = 0\}. \quad (20)$$

That is, H_p consists of all vectors tangent to S^3 at p that are orthogonal to p when p is viewed as a radius-vector in \mathbb{C}^2 . One can define the connection 1-form \mathcal{A} on S^3 as follows:

$$\mathcal{A} = 2g(\bar{z}_1 dz_1 + \bar{z}_2 dz_2), \quad (21)$$

where g is a scaling factor. Indeed, action of a form on arbitrary complex vector (v_1, v_2) produces its vertical component:

$$2g(\bar{z}_1 dz_1 + \bar{z}_2 dz_2)(v_1, v_2) = 2g(\bar{z}_1 v_1 + \bar{z}_2 v_2) \quad (22)$$

and $g = 1/2$ for the case of Hopf fibration (compare with (18)). We will keep this factor to generalize our considerations later on. Expanding the connection form in terms of real and imaginary parts, we get

$$\mathcal{A} = 2g \operatorname{Re}(\bar{z}_1 dz_1 + \bar{z}_2 dz_2) + 2ig \operatorname{Im}(\bar{z}_1 dz_1 + \bar{z}_2 dz_2). \quad (23)$$

However, since $(z_1, z_2) \in S^3$, $|z_1|^2 + |z_2|^2 = 1$, we have

$$2 \operatorname{Re}(\bar{z}_1 dz_1 + \bar{z}_2 dz_2) = d(|z_1|^2 + |z_2|^2) = 0, \quad (24)$$

and thus,

$$\mathcal{A} = 2ig \operatorname{Im}(\bar{z}_1 dz_1 + \bar{z}_2 dz_2). \quad (25)$$

Finally, expanding $z_1 = x_1 + ix_2$, and $z_2 = x_3 + ix_4$ we can express A as

$$\mathcal{A} = 2g(x_1 dx_2 - x_2 dx_1 + x_3 dx_4 - x_4 dx_3), \quad (26)$$

where x_i represent the real components of the vector in \mathbb{R}^4 .

Let us illustrate the action of this form in coordinates and consider the vertical and horizontal subspaces for the particular example of the Hopf fibration. Consider, at $p = (z_1, z_2) \in S^3$, the following orthonormal basis of tangent vectors to S^3 :

$$u_v = -x_2 \partial_1 + x_1 \partial_2 - x_4 \partial_3 + x_3 \partial_4, \quad (27)$$

$$\begin{aligned} u_{h1} &= -x_3 \partial_1 + x_4 \partial_2 + x_1 \partial_3 - x_2 \partial_4, \\ u_{h2} &= -x_4 \partial_1 - x_3 \partial_2 + x_2 \partial_3 + x_1 \partial_4, \end{aligned} \quad (28)$$

where a physicist can think about ∂_i as unit basis vectors $\partial_i \leftrightarrow \mathbf{e}_i$ (in this particular case). Then, for a vector u_v starting at $p = (x_1, x_2, x_3, x_4)$ and ending at

$$h(t) = (x_1 - tx_2, x_2 + tx_1, x_3 - tx_4, x_4 + tx_3), \quad (29)$$

we obtain

$$h(t) = (1 + it)p = ((1 + it)z_1, (1 + it)z_2) = (\alpha z_1, \alpha z_2) \quad (30)$$

which means that this vector indeed belongs to the vertical space (19). Otherwise, one can directly write the action of the 1-form (26) on (27): Using that $dx_j(\partial_k) = \delta_{jk}$, we have:

$$\mathcal{A}(u_v) = 2g(x_1^2 + x_2^2 + x_3^2 + x_4^2) = 2g, \quad (31)$$

since the point lies on the unit 3-sphere. For completeness, one can also verify that for the two other tangent vector fields (28) the form gives

$$\mathcal{A}(u_3) = \mathcal{A}(u_4) = 0, \quad (32)$$

which confirms that only u_v has a nonzero projection on the vertical subspace, and u_{h1} and u_{h2} are horizontal vector fields.

2.1.4 Horizontal lift and holonomy

In this section, we introduce the definitions that are likely the most important for understanding the Berry phase. Let (E, B, π, F) be a smooth fibre bundle, where E is the total space (S^3 in our case), B is the base space (Poincaré sphere S^2 in our case), $\pi: E \rightarrow B$ is the projection map, and F is the fibre. Let $v \in T_x B$ be a tangent vector at $x \in B$, and let $p \in E$ be a point such that $\pi(p) = x$. The **horizontal lift** of some vector v at p is the unique vector $\tilde{v} \in T_p E$ satisfying the following conditions:

1. Projection preservation: The vector \tilde{v} projects to v under the pushforward of π , i.e.,

$$\pi_*(\tilde{v}) = v, \quad (33)$$

where $\pi_*: T_p E \rightarrow T_x B$.

2. Horizontality The vector \tilde{v} lies in the horizontal subspace $H_p \subset T_p E$, defined by the connection form \mathcal{A} , i.e.,

$$\mathcal{A}_p(\tilde{v}) = 0. \quad (34)$$

The *horizontal lift* γ of a curve γ_0 on the base space is defined as follows: the projection of a lifted curve should be the initial curve, and its tangent vector should be the horizontal lift of the tangent vector to the initial curve. In Fig. 2 the horizontal lift of the curve on the base space is depicted with light blue as well as lifts of tangent vectors. In the Appendix C.1 we provide an example in coordinates.

However, if the path on the base space is closed, the lifted path is, in general, not closed: one arrives at a different point on the fiber, as shown in the figure. This difference is called **holonomy** of the connection, and corresponds exactly to the geometric phase [19, 39]! An example is also given in Appendix C.1. In principle, holonomy can be introduced without the notion of curvature, but for both theoretical and computational purposes, additional concepts are often employed. We briefly discuss them in the Appendix C.3.

The last definition is *parallel transport*. For a point $p \in E$, it is simply the motion of this point along a horizontally lifted curve.

2.1.5 Action of the waveplate

As we have seen earlier, action of the waveplate is described with help of $SU(2)$ matrix (9). But how can we see that this action corresponds somehow to the connection form (26)? We discuss this in detail in the Appendix C.3. The answer is the following: the motion of a point on the sphere S^3 under the action (9) of an $SU(2)$ one-parameter subgroup comes from parallel transport if and only if the corresponding projection on the Poincaré sphere moves along a great circle, namely, a geodesic on S^2 [4, 40, 41].

3 Vortex beams. Main result.

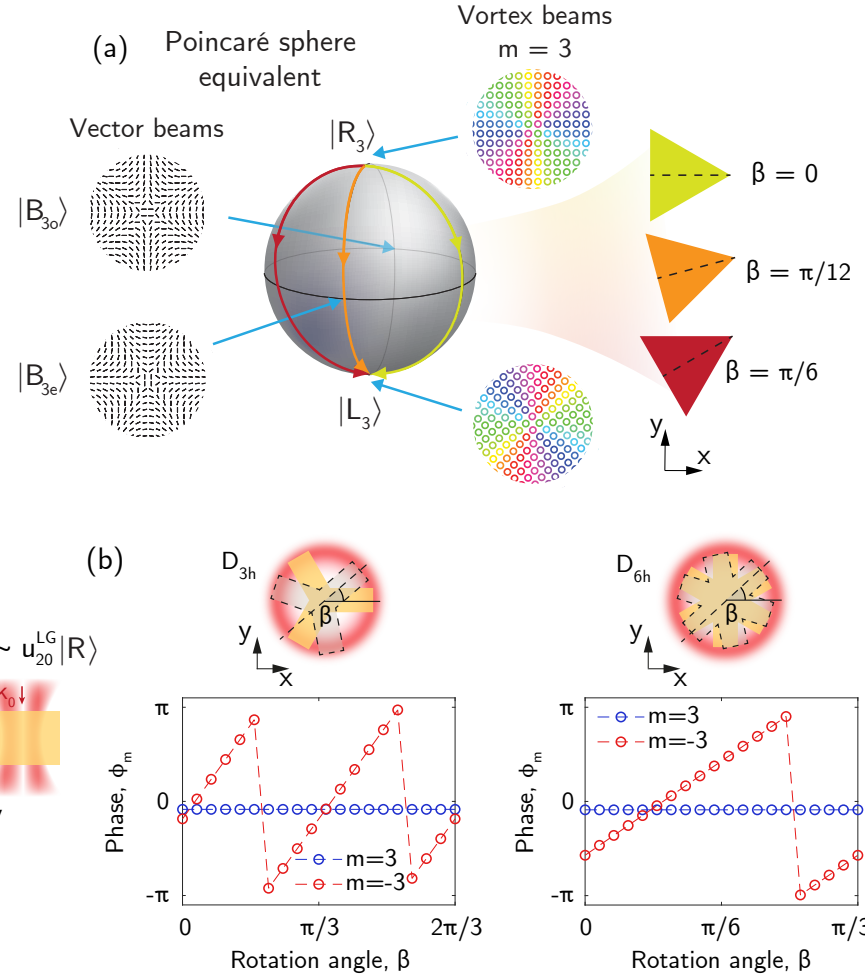


Figure 3: (a) Geometry of the experiment involving the transmission of vortex beams with total angular momentum projection m through a prism with n -fold rotational symmetry. This setup is fully analogous to the one depicted in Fig. 1, but different β is required. (b) Numerically calculated phase acquired by the rotation of nanoparticles with D_{3h} and D_{6h} symmetries under excitation by a vortex beam ($m = 3$), the condition $2m = n\nu$ is satisfied. In both cases 2π phase accumulated by $\pi/3$ rotation.

Let us now consider vortex beams. In cylindrical coordinates, vortex beams allow for the construction of a higher-order Poincaré sphere [15, 42], which is fully analogous to the usual one:

$$|R_m\rangle \sim e^{im\varphi}(\hat{\rho} + i\hat{\varphi}), \quad (35)$$

$$|L_m\rangle \sim e^{-im\varphi}(\hat{\rho} - i\hat{\varphi}), \quad (36)$$

where $|R_m\rangle$ and $|L_m\rangle$ signify right- and left-handed vortex beams, respectively, with $m \in \mathbb{Z}$ denoting the total angular momentum (TAM) projection, φ the azimuthal angle, and $\hat{\rho}$, $\hat{\varphi}$ are the unit vectors of cylindrical coordinate system. The equivalence sign \sim stands for the symmetry behavior, i.e. behavior under rotations around the z-axis. A detailed discussion

can be found in [43]. Note, that

$$(\hat{\mathbf{x}} \pm i\hat{\mathbf{y}}) = e^{\pm i\varphi} (\hat{\boldsymbol{\rho}} \pm i\hat{\boldsymbol{\varphi}}), \quad (37)$$

and the sign refers to the polarization (helicity) here. We omit the dependence of the radial coordinate r [44], since it does not alter the general symmetry we are interested in. Similarly,

$$\mathbf{E} = c_1 |R_m\rangle + c_2 |L_m\rangle. \quad (38)$$

At this stage we want to describe an experiment, what would be analogous to the one with the waveplate. A vortex beam is fundamentally different from a plane wave, being anisotropic in transverse direction. However, it is well-known that for a plane wave not only waveplates, but metasurfaces with rectangular blocks as metaatoms are widely used [2, 9, 45–47]. Indeed, each metaatom has, *e.g.*, C_{2v} , D_{2h} or C_{1h} symmetry. For these symmetries, two eigenmodes, one of which is excited with an x - and the second with an y -polarized wave, are transformed according to the different irreducible representations, and, as a consequence, have different resonance frequencies and excited with different phases [24, 43]. This consideration via the eigenmodes and irreps may appear too complicated for this simple case of rectangular block; however, it can be easily adapted to the vortex beam case. Indeed, vector beams, which are defined as:

$$|B_{me}\rangle \propto |L_m\rangle + |R_m\rangle \quad (39)$$

$$|B_{mo}\rangle \propto |L_m\rangle - |R_m\rangle, \quad (40)$$

where the indexes e and o denote the parity under reflection in $y = 0$ plane, refer to the endpoints of a diameter of the higher-order Poincaré sphere. They serve as an analogy for vertical and horizontal linear polarization in the plane wave case. Thus, instead of the rectangular block, one should use the nanostructure, in which $|B_{me}\rangle$ and $|B_{mo}\rangle$ are transformed according to the different irreps. This metaatom should have C_{nv} or D_{nh} symmetry with $2m = n\nu$, $\nu \in \mathbb{Z}$ (See also [43], Section 8). For such a structure, these vector beams will excite eigenmodes which have different phases, leading to exactly the same process previously discussed. Note that this process is not perfect because other values of m are also obtained during scattering. Since one cannot avoid them, the only way out is to tailor the geometry so as to minimize their contribution. Though being analogous to the simplest case, this process presents only one difference. In order to obtain the same phase difference δ one should rotate the nanostructure by a smaller angle β (see Fig. 1a). One can also notice that opposite points on the diameter refer to the beam rotation by $\beta = \pi/(2m)$, as well as the nanostructure rotation for the opposite paths on the Poincaré sphere. For a plane wave $m = \pm 1$. To our knowledge, this analogy was never noticed before.

Let us also note that, in principle, if we have an incident wave with TAM projection m^{inc} and an output wave of the same frequency as the TAM projection m^{out} , the acquired phase will be equal to [48]

$$\phi(\beta) = (m^{\text{out}} - m^{\text{inc}})\beta, \quad (41)$$

however, the corresponding geometric interpretation is not straightforward for other $|m^{\text{out}}| \neq |m^{\text{inc}}|$. Moreover, in view of the selection rules for scattering, only $m^{\text{out}} = m^{\text{inc}} + n\mathbb{Z}$ are allowed.

Figure 3b shows numerical calculation of geometric phase for particles of different symmetries illuminated by a beam with $m = 3$ featuring second order phase singularity (LG mode with $l = 2$, $p = 0$, see Sec. F). One can see that both D_{3h} and D_{6h} particles with the same input, provide a 2π phase winding of the cross polarized component under rotation by the angle $\pi/3$.

3.1 Vortex beams via the Hermite-Gaussian sphere

Let us now proceed to another experiment, which is commonly associated with the geometric phase of optical beams. This experiment possesses a completely different geometry, when compared to the one described above. First, we consider only the scalar part of the beam, because polarization may be considered independently for this experiment. Here we will use the paraxial approximation. In the previous case, no such an approximation was needed. The Hermite-Gaussian modes are solutions of the paraxial wave equation [49–51]

$$\frac{\partial^2}{\partial x^2}u(\mathbf{r}) + \frac{\partial^2}{\partial y^2}u(\mathbf{r}) = -2ik\frac{\partial}{\partial z}u(\mathbf{r}). \quad (42)$$

which may be written as

$$u_{\nu\eta}^{\text{HG}}(\mathbf{r}) = \frac{1}{\gamma}\psi_{\nu}\left(\frac{x}{\gamma}\right)\psi_{\eta}\left(\frac{y}{\gamma}\right)\exp\left[\frac{\text{i}kr_t^2}{2R} - \text{i}\chi(\nu + \eta + 1)\right], \quad (43)$$

where $\psi_n(\xi)$ are the normalized Hermite functions corresponding to the one-dimensional harmonic oscillator:

$$\psi_n(\xi) = [2^n n! \sqrt{\pi}]^{-1/2} \exp\left(-\frac{\xi^2}{2}\right) H_n(\xi). \quad (44)$$

$\chi = \chi(z)$ is the Gouy phase, $\gamma = \gamma(z)$ is the spot radius and $R = R(z)$ is the radius of the curvature of the wavefront, $\eta, \nu \in \mathbb{N}_0$, k is a wavenumber, $r_t = x^2 + y^2$, $H_n(\xi)$ is Hermite polynomial [50]. The solutions can be also presented in a different form:

$$u_{lp}^{\text{LG}}(\mathbf{r}) = \exp\left[\frac{ik}{2R}r_t^2 - \text{i}\chi(N + 1)\right] \frac{1}{\gamma}\psi_{lp}\left(\frac{x}{\gamma}, \frac{y}{\gamma}\right), \quad (45)$$

$$\psi_{lp} = e^{\text{i}l\varphi} \exp\left(-r^2/2\gamma^2\right) r^{|l|} L_p^{|l|}\left(r^2/\gamma^2\right), \quad (46)$$

where $N = \eta + \nu = 2p + |l|$ and $L_p^{|l|}$ is the generalized Laguerre polynomial. Notice that there are $N + 1$ solutions for each N . For our purposes, an exact form is not necessary, because we are only interested in the following presentation [50, 52, 53]:

$$u_{\nu\eta}^{\text{HG}}(\mathbf{r}) = \frac{1}{\sqrt{\nu!\eta!}} \left(\hat{a}_x^{\dagger}\right)^{\nu} \left(\hat{a}_y^{\dagger}\right)^{\eta} u_{00}(\mathbf{r}) \quad (47)$$

where

$$\hat{a}_x = \frac{1}{\sqrt{2bk}} \left[kx + (b + iz)\frac{\partial}{\partial x} \right], \quad (48)$$

$$\hat{a}_x^{\dagger} = \frac{1}{\sqrt{2bk}} \left[kx - (b - iz)\frac{\partial}{\partial x} \right]. \quad (49)$$

and \hat{a}_y is defined analogously with $x \rightarrow y$ [50, 52], b is the Rayleigh range, $\chi(z) = \arctan(z/b)$, and $\frac{1}{b+iz} = \frac{1}{k\gamma^2} - \frac{\text{i}}{R}$ [50]. Let us define the operators [54–56]

$$L_x = \frac{1}{2}(\hat{a}_x^{\dagger}\hat{a}_x - \hat{a}_y^{\dagger}\hat{a}_y) = \frac{1}{4bk} [k^2(x^2 - y^2) + 2ikz(x\partial_x - y\partial_y) - (b^2 + z^2)(\partial_x^2 - \partial_y^2)]. \quad (50)$$

$$L_y = \frac{1}{2}(\hat{a}_x^{\dagger}\hat{a}_y + \hat{a}_y^{\dagger}\hat{a}_x) = \frac{1}{2bk} [k^2xy + ikz(x\partial_y + y\partial_x) - (b^2 + z^2)\partial_x\partial_y] \quad (51)$$

$$L_z = \frac{1}{2\text{i}}(\hat{a}_x^{\dagger}\hat{a}_y - \hat{a}_y^{\dagger}\hat{a}_x) = \frac{\text{i}}{2} (y\partial_x - x\partial_y) \quad (52)$$

$$L_0 = \frac{1}{2}(\hat{a}_x^\dagger \hat{a}_x + \hat{a}_y^\dagger \hat{a}_y) = \frac{1}{4bk} [k^2(x^2 + y^2) + 2ikz(x\partial_x + y\partial_y) - 2k(b - iz) - (b^2 + z^2)(\partial_x^2 + \partial_y^2)]. \quad (53)$$

For $z = 0$ we have [56]

$$L_x u_{\nu\eta}^{HG}(\mathbf{r}) = \frac{1}{2}(\nu - \eta) u_{\nu\eta}^{HG}(\mathbf{r}), \quad (54)$$

and introducing

$$\hat{a}_\pm^\dagger = \frac{\hat{a}_x^\dagger \pm i\hat{a}_y^\dagger}{\sqrt{2}}, \quad (55)$$

we get

$$u_{lp}^{LG}(\mathbf{r}) = \frac{1}{\sqrt{\nu_+! \nu_-!}} \left(\hat{a}_+^\dagger \right)^{\nu_+} \left(\hat{a}_-^\dagger \right)^{\nu_-} u_{00}(\mathbf{r}), \quad (56)$$

$$L_z u_{lp}^{LG}(\mathbf{r}) = \frac{1}{2}(\nu_+ - \nu_-) u_{lp}^{LG}(\mathbf{r}). \quad (57)$$

where $l = \nu_+ - \nu_-$, $p = \min(\nu_+, \nu_-)$.

Let us imagine an experiment, which would change the “relative phase” δ between \hat{a}_x^\dagger and \hat{a}_y^\dagger . This would mean, that $u_{\nu\eta}^{HG}(\mathbf{r})$ will acquire some additional relative phase equal to $(\nu - \eta)\delta/2$. This can be realized with the mode converter ([53], eq. (20)-(22), [57]). Thus,

$$u_{lp}^{LG}(\mathbf{r}) = \frac{1}{\sqrt{\nu_+! \nu_-!}} \frac{\left(\hat{a}_x^\dagger + i\hat{a}_y^\dagger \right)^{\nu_+}}{\sqrt{2}} \frac{\left(\hat{a}_x^\dagger - i\hat{a}_y^\dagger \right)^{\nu_-}}{\sqrt{2}} u_{00}(\mathbf{r}), \quad (58)$$

transforms into

$$u_{lp}^{LG}(\mathbf{r}) = \frac{1}{\sqrt{\nu_+! \nu_-!}} \frac{\left(e^{i\delta/2} \hat{a}_x^\dagger + i e^{-i\delta/2} \hat{a}_y^\dagger \right)^{\nu_+}}{\sqrt{2}} \frac{\left(e^{i\delta/2} \hat{a}_x^\dagger - i e^{-i\delta/2} \hat{a}_y^\dagger \right)^{\nu_-}}{\sqrt{2}} u_{00}(\mathbf{r}), \quad (59)$$

Let us note, that in each multiplier, \hat{a}_i^\dagger behaves just in the same way as E_i in previous waveplate considerations. Thus, one can depict all the states on the Hermite-Laguerre sphere, which would be a Poincaré-like sphere, constructed for creation operators. One can also consider a fiber bundle associated with such a sphere. Note that it is important, that all the multipliers behave identically. On the one side, just by comparison with a half-waveplate, one may consider the 3-sphere S^3 , associated with complex numbers (c_1, c_2) , associated with “state” Φ , which describes the phases of the creation operators:

$$\Phi = c_1 \hat{a}_+^\dagger + c_2 \hat{a}_-^\dagger \quad (60)$$

$$|c_1|^2 + |c_2|^2 = 1. \quad (61)$$

For the case of two operators, the geometry is just the same as in the simplest case. However, one should keep in mind that each point on the operator 2-sphere would correspond to some state of the beam (59), which we want to be a point in the total space, so the fiber coordinate corresponds to the phase of the beam. From the (59), the common phase turns out to be a phase $(\nu_+ - \nu_-)\alpha = l\alpha$, where α corresponds to the “phase” of the operators Φ .

Thus, points of a fibre whose phases α differ by $2\pi/l$ should be considered equivalent, and giving rise to an orbifold (lens space $L_{l,1}$) [58, 59], which also corresponds to the monopole of charge l [60]. The connection form has a similar form, but with multiplier $g = l/2$ in (21). Polarisation is considered independently, and modified, as before, via the waveplate. The final geometric phase, and order of the Lens space will be characterised in this case with the total angular momentum projection $m = l + 1$.

3.2 Majorana representation

Let us write again the relations between different indices, and introduce J and μ :

$$\mu = \ell/2, \quad J = N/2, \quad (62)$$

$$J + \mu = (N + |\ell|)/2 = \ell + p, \quad (63)$$

$$J - \mu = (N - |\ell|)/2 = p \quad (64)$$

And and express the state (56) as follows [61–65]:

$$|J, \mu\rangle = \frac{(a_+^\dagger)^{J+\mu}}{\sqrt{(J+\mu)!}} \frac{(a_-^\dagger)^{J-\mu}}{\sqrt{(J-\mu)!}} |0, 0\rangle. \quad (65)$$

Let us consider an arbitrary beam:

$$|\Psi\rangle = \sum_{\mu=-J}^J c_\mu |J, \mu\rangle = \sum_{\mu=-J}^J c_\mu \frac{(a_+^\dagger)^{J+\mu} (a_-^\dagger)^{J-\mu}}{\sqrt{(J+\mu)! (J-\mu)!}} |0, 0\rangle, \quad (66)$$

or, equivalently

$$|\Psi\rangle = \sum_{\mu=-J}^J c_\mu \frac{(a_+^\dagger)^{J+\mu} (a_-^\dagger)^{-(J+\mu)}}{\sqrt{(J+\mu)! (J-\mu)!}} (a_-^\dagger)^{2J} |0, 0\rangle. \quad (67)$$

Let z_i be the roots of the polynomial of a power $2J$ in the variable x (formally one can consider $(a_+^\dagger)(a_-^\dagger)^{-1}$ as x in (67)) and with index shift $J + \mu = i$:

$$\sum_{i=0}^{2J} c_{i-J} \frac{x^i}{\sqrt{(2J-i)! i!}} = 0 \leftrightarrow \frac{c_J}{\sqrt{(2J)!}} \prod_{i=1}^{2J} (x + z_i) = 0. \quad (68)$$

Keeping in mind the fundamental theorem of algebra, one can also write (67) in the same form:

$$|\Psi\rangle = c_J \sqrt{\frac{1}{(2J)!}} \prod_{i=1}^{2J} (a_+^\dagger + z_i a_-^\dagger) |0, 0\rangle. \quad (69)$$

Thus, we have a correspondence between coefficients c_μ and roots z_i , which can be depicted on sphere S^2 with the help of stereographic projection. For Laguerre-gaussian beam only one c_{μ_0} is non-zero, thus we have $J + \mu_0$ roots $z_i = 0$, and $J - \mu_0$ at the infinity. The action of the mode converter rotates the roots collectively.

4 Discussion

We wish to point out that in the literature the term *geometric phase* is not always used consistently. In particular, while for a wave plate the trajectory on the Poincaré sphere is clearly defined and can be parametrized by a real coordinate, this is no longer the case for the corresponding nanoparticle. In a nanoparticle, the polarization cannot be always defined or tracked inside the structure in the same way as in a waveplate, and the associated unitary matrices are therefore introduced in a rather formal sense. Nevertheless, for nanoparticles, the phase can be obtained by a different procedure, namely by rotating the particle and moving to a different reference frame.

For the so-called nonlinear geometric phase, there exists an analogy with this approach [66], however, in this case it is apparently no longer possible, even formally, to introduce a unitary matrix or a closed path on the Poincaré sphere. This raises the question of whether all these phases should indeed be termed geometric, or whether the concept of geometric phase should be extended to a broader class of problems. We regard the strict delineation of this class of phases in optics as an open question for discussion.

We further propose to reserve the term *Pancharatnam-Berry phase* exclusively for phases whose geometry coincides with that described here and is associated with the Hopf fibration. Other phases, for example, the frequently used illustration (Fig. 4) based on parallel transport of a tangent vector on a sphere are indeed geometric phases, but they can be misleading when used in discussions of the Pancharatnam–Berry phase, as they are characterized by a fundamentally different geometry.

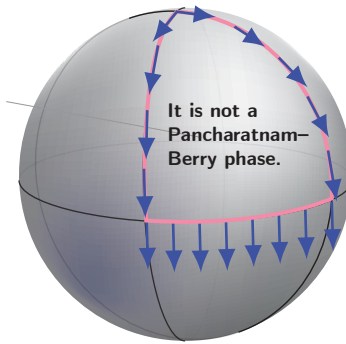


Figure 4: A frequently used illustration of a geometric phase which, however, is not a Pancharatnam-Berry phase and has a different geometry; it is equal to the full solid angle rather than half of it.

Another open issue concerns the non-uniqueness of the connection. The connection discussed here is the canonical one, however, it is in principle possible to introduce other connections that are not related to it by a gauge transformation and that yield different curvature and different holonomy, while still corresponding to the same Chern class. To our knowledge, such situations have not been discussed in the optics literature. Nevertheless, it cannot be excluded that for other physical problems precisely these alternative connections may turn out to be relevant. It might then be expedient to resort to the classical complex algebraic-geometric formalism employed in [67, 68]. On the experimental side, some of the theoretical issues discussed in [69] may be also fruitfully explored.

5 Conclusions

Summing up, in this paper we have analyzed the geometric (Pancharatnam) phase, starting from its abstract mathematical definition and establishing an explicit bridge to physical observables through concrete calculations. We have further demonstrated that for vortex beams, an entirely analogous Berry phase can be introduced, which is equal to $\Omega/2$, rather than $\ell\Omega/2$, within a distinct experimental configuration. The underlying geometry of both situations has been described in detail, emphasizing the common structure behind their phase evolution.

6 Acknowledgements

K.F. thanks Timur Seidov, Tim Sulimov, Igor Shenderovich, Nikita Belousov, Costantino de Angelis for the fruitful discussions. Part of this work was conducted at the University of Brescia. K.F. gratefully acknowledges support from the Alexander von Humboldt Foundation.

E.M. acknowledges the PNRR RESTART project Smart Metasurfaces Advancing Radio Technology (SMART), CUP E63C22002040007, and Erasmus Mundus EMIMEP, CUP D81I24000080006.

M.S. thanks Gabriele Barbieri for enlightening discussions and collaboration on related topics. His research is supported by UCSC D1-funds and it has been carried out within INDAM-GNSAGA's framework.

A Stereographic Projection

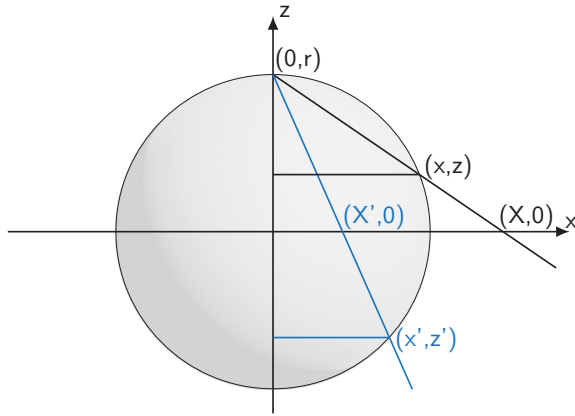


Figure 5: Stereographic projection establishes a one-to-one correspondence between the points on the sphere and those on the plane.

Let the center of a sphere of radius r be at $(0, 0, 0)$. Draw a line from the north pole that intersects the sphere and the plane $z = 0$ at (x, y, z) and $(X, Y, 0)$, respectively. We establish a relationship between the coordinates. From the similarity of triangles,

$$X = \frac{rx}{r-z}, \quad Y = \frac{ry}{r-z}. \quad (70)$$

However, we would like to express the sphere coordinates in terms of the plane coordinates. For this, we consider the plane as a complex plane and introduce

$$Z = \frac{r(x+iy)}{r-z}, \quad \bar{Z} = \frac{r(x-iy)}{r-z}. \quad (71)$$

Consider

$$Z\bar{Z} = \frac{r^2(x^2+y^2)}{(r-z)^2} = \frac{r^2(r^2-z^2)}{(r-z)^2} = \frac{r^2(r+z)}{(r-z)}, \quad (72)$$

from here

$$z = \frac{r(Z\bar{Z} - r^2)}{(Z\bar{Z} + r^2)}, \quad (73)$$

$$x = \frac{X(r-z)}{r} = \frac{(Z+\bar{Z})(r-z)}{2r} = \frac{r^2(Z+\bar{Z})}{(Z\bar{Z} + r^2)}, \quad (74)$$

$$y = \frac{Y(r-z)}{r} = \frac{-ir^2(Z-\bar{Z})}{(Z\bar{Z}+r^2)} \quad (75)$$

Thus, every point on the sphere, except the north pole, corresponds to a point on the plane. The extended plane includes the point at infinity, which corresponds to the north pole. Stereographic projection preserves angles and generalized circles; that is, it maps circles on the sphere to circles or straight lines on the plane.

B Projective space

One can also find a detailed explanation and relation to the Poincaré sphere in [23]. The complex projective space \mathbb{CP}^n is the quotient set $\mathbb{C}^{n+1} \setminus \{0\}$ with respect to the equivalence relation

$$x \sim y \Leftrightarrow \exists \lambda \in \mathbb{C} \setminus \{0\} : x = \lambda y \quad (76)$$

$$\mathbb{CP}^n = (\mathbb{C}^{n+1} \setminus \{0\}) / \sim \quad (77)$$

One can often encounter notations like $\mathbb{C} \setminus \{0\} := \mathbb{C}^*$. The complex projective line \mathbb{CP}^1 is homeomorphic to a sphere, which is also called Riemann sphere. In other words, the Riemann sphere can be defined as the set of all lines passing through the origin in \mathbb{C}^2 . Any point on the Riemann sphere can be represented by a pair of complex numbers (z_1, z_2) , and two points (z_1, z_2) and (w_1, w_2) represent the same point on the Riemann sphere if there exists a nonzero complex number λ such that:

$$(z_1, z_2) = \lambda(w_1, w_2). \quad (78)$$

This equivalence relation introduces the concept of projective coordinates on the Riemann sphere, typically denoted as $[z_1 : z_2]$. The complex plane \mathbb{C} corresponds to the subset of the Riemann sphere where $z_2 \neq 0$, and each point $z \in \mathbb{C}$ is identified with the point $[z_1/z_2 : 1] = [z : 1]$ on the Riemann sphere. The point at infinity is represented by $[1 : 0]$.

C Derivations for the SU(2) matrix for the rotated waveplate

The optical axis of the waveplate is rotated by an angle β with respect to the x-axis. We can introduce new $E_{x'}$ and $E_{y'}$ in another coordinate system along the symmetry planes of the waveplate. In general case it is

$$E_x = \cos \beta E_{x'} + \sin \beta E_{y'}, \quad E_y = -\sin \beta E_{x'} + \cos \beta E_{y'} \quad (79)$$

The initial circularly polarized wave is expressed through the new coordinates as

$$E_R = e^{i\beta} \frac{E_{x'} - iE_{y'}}{\sqrt{2}}, \quad E_L = e^{-i\beta} \frac{E_{x'} + iE_{y'}}{\sqrt{2}} \quad (80)$$

$$E_{x'} = \frac{e^{-i\beta} E_R + e^{i\beta} E_L}{\sqrt{2}}, \quad E_{y'} = -\frac{e^{-i\beta} E_R - e^{i\beta} E_L}{i\sqrt{2}} \quad (81)$$

Therefore for electric field components transmitted through a rotated waveplate we have:

$$\tilde{E}_R = e^{i\beta} \left(e^{i\delta/2} \frac{e^{-i\beta} E_R + e^{i\beta} E_L}{2} + i e^{-i\delta/2} \frac{e^{-i\beta} E_R - e^{i\beta} E_L}{2i} \right) \quad (82)$$

$$\tilde{E}_L = e^{-i\beta} \left(e^{i\delta/2} \frac{e^{-i\beta} E_R + e^{i\beta} E_L}{2} - i e^{-i\delta/2} \frac{e^{-i\beta} E_R - e^{i\beta} E_L}{2i} \right) \quad (83)$$

$$\tilde{E}_R = \left(e^{i\delta/2} \frac{E_R + e^{2i\beta} E_L}{2} + e^{-i\delta/2} \frac{E_R - e^{2i\beta} E_L}{2} \right) \quad (84)$$

$$\tilde{E}_L = \left(e^{i\delta/2} \frac{e^{-2i\beta} E_R + E_L}{2} - e^{-i\delta/2} \frac{e^{-2i\beta} E_R - E_L}{2} \right) \quad (85)$$

$$\begin{pmatrix} \tilde{E}_L \\ \tilde{E}_R \end{pmatrix} = \begin{pmatrix} \cos \delta/2 & ie^{-2i\beta} \sin \delta/2 \\ ie^{2i\beta} \sin \delta/2 & \cos \delta/2 \end{pmatrix} \begin{pmatrix} E_L \\ E_R \end{pmatrix} \quad (86)$$

So we get the general formula:

$$\begin{pmatrix} \tilde{E}_L \\ \tilde{E}_R \end{pmatrix} = (\mathbb{I} \cos \delta/2 + i(\cos 2\beta \sigma_x + \sin 2\beta \sigma_y) \sin \delta/2) \begin{pmatrix} E_L \\ E_R \end{pmatrix}. \quad (87)$$

C.1 Horizontal lift and holonomy: an example

For more general considerations see also the book [35]. Let \mathcal{A} be the global $U(1)$ connection 1-form on S^3 . For a lifted curve $z(t) \in S^3 \subset \mathbb{C}^2$ the horizontality is

$$\mathcal{A}(\dot{z}(t)) = 0. \quad (88)$$

Here we use $z = (z_1, z_2)$ with $z_1 = x_1 + ix_2$, $z_2 = x_3 + ix_4$. Let us fix any (not necessarily horizontal, preferably closed) reference lifted curve $z_{\text{ref}}(t)$ with the same base projection. Any other lift differs by a fibre rotation $e^{-i\alpha(t)}$, hence

$$z(t) = e^{-i\alpha(t)} z_{\text{ref}}(t), \quad \dot{z} = e^{-i\alpha(t)} (\dot{z}_{\text{ref}} - i\dot{\alpha} z_{\text{ref}}). \quad (89)$$

Using the $U(1)$ -invariance of \mathcal{A} and $\mathcal{A}(v_V) = 1$, the horizontality condition (88) with (89) gives

$$0 = \mathcal{A}(\dot{z}) = \mathcal{A}(\dot{z}_{\text{ref}}) - \dot{\alpha}(t) \implies \dot{\alpha}(t) = \mathcal{A}(\dot{z}_{\text{ref}}(t)). \quad (90)$$

In real coordinates on $S^3 \subset \mathbb{R}^4$ we use

$$\mathcal{A} = x_1 dx_2 - x_2 dx_1 + x_3 dx_4 - x_4 dx_3, \quad \mathcal{A}(\dot{x}) = x_1 \dot{x}_2 - x_2 \dot{x}_1 + x_3 \dot{x}_4 - x_4 \dot{x}_3. \quad (91)$$

Now we consider the example of the closed curve on the Poincaré sphere with a fixed θ and denote $a = \cos(\theta/2)$, $b = \sin(\theta/2)$. A convenient (non-horizontal) closed reference lift of this parallel is given by

$$x_{\text{ref}}(t) = (a, 0, b \cos \varphi(t), -b \sin \varphi(t)), \quad (92)$$

whose Hopf projection is the latitude (parallel) on S^2 with $Z = \cos \theta$. Indeed, $z_1(t) = a$, $z_2(t) = b \cos \varphi(t) - ib \sin \varphi(t) = b e^{-i\varphi(t)}$, and using the Hopf map (16) we obtain $z_1 \bar{z}_2 = a \cdot b e^{i\varphi(t)}$,

$$\pi(z_{\text{ref}}(t)) = (\sin \theta \cos \varphi(t), \sin \theta \sin \varphi(t), \cos \theta).$$

Along this curve the connection form evaluates to

$$\mathcal{A}(\dot{x}_{\text{ref}}(t)) = -b^2 \dot{\varphi}(t) = -\sin^2 \frac{\theta}{2} \dot{\varphi}(t) = -\frac{1}{2}(1 - \cos \theta) \dot{\varphi}(t). \quad (93)$$

Therefore, the horizontality equation (90) gives

$$\dot{\alpha}(t) = \mathcal{A}(\dot{x}_{\text{ref}}(t)) = -\frac{1}{2}(1 - \cos \theta) \dot{\varphi}(t). \quad (94)$$

For a closed loop along the parallel, φ increases by 2π , hence

$$\Delta\alpha = -\frac{1}{2} \int_0^{2\pi} (1 - \cos\theta) d\varphi = -\pi(1 - \cos\theta), \quad \text{Hol} = \exp(i\Delta\alpha). \quad (95)$$

Since the solid angle of the spherical cap bounded by the parallel is $\Omega = 2\pi(1 - \cos\theta)$, we have the equivalent relation

$$\Delta\alpha \equiv -\frac{1}{2}\Omega, \quad \text{Hol} = \exp(-i\frac{\Omega}{2}). \quad (96)$$

Note that we could consider a different reference lift, e.g.

$$x_{\text{ref}}(t) = \left(a \cos \frac{\varphi(t)}{2}, a \sin \frac{\varphi(t)}{2}, b \cos \frac{\varphi(t)}{2}, -b \sin \frac{\varphi(t)}{2} \right), \quad (97)$$

and this one is not closed. This means that one should add an additional phase, in this case, π , which corresponds to the non-closedness of the reference lift. This is related to the part of the phase that is referred to as dynamical in [70].

C.2 Global and local descriptions

In practical applications one usually does not work directly with the global connection form \mathcal{A} on the total space E , but rather with its local representatives on the base manifold. This step is often left implicit, but it is important to state it explicitly: obtaining a local connection on the base requires the choice of a local section of the fibre bundle. We introduce angular coordinates on the S^3 (θ, φ, ψ) with $\theta \in [0, \pi]$ and $\varphi, \psi \in [0, 2\pi]$, and write [34]

$$z_1 = \cos \frac{\theta}{2} \exp \left(i \frac{\psi + \varphi}{2} \right), \quad (98)$$

$$z_2 = \sin \frac{\theta}{2} \exp \left(i \frac{\psi - \varphi}{2} \right). \quad (99)$$

The projection $\pi: S^3 \rightarrow S^2$ given by the Hopf map gives

$$x = \sin \theta \cos \varphi, \quad y = \sin \theta \sin \varphi, \quad z = \cos \theta, \quad (100)$$

which is the standard spherical parametrization of S^2 . The angles (θ, φ) therefore parametrize the base $B = S^2$, while ψ parametrizes the fibre $F = S^1$.

To pass from the global connection on E to a local gauge potential on B , we need a local section. A (local) section is a smooth map

$$s: U \subset B \rightarrow E \quad (101)$$

such that $\pi \circ s = \text{id}_U$. For the Hopf bundle we use the canonical sections

$$f_N(\theta, \varphi) = (\theta, \varphi, \psi = -\varphi), \quad (102)$$

$$f_S(\theta, \varphi) = (\theta, \varphi, \psi = +\varphi), \quad (103)$$

defined on the coordinate patches $U_N = S^2 \setminus \{\text{south pole}\}$, $U_S = S^2 \setminus \{\text{north pole}\}$, respectively, so that each section is smooth on its domain.

Given a connection 1-form \mathcal{A} on E , its local representative on $U \subset B$ is obtained as a pullback along a chosen section s . Let $s: B \rightarrow E$ be a smooth map and let α be a 1-form on E . The **pullback** of the 1-form α , denoted by $s^*\alpha$, is the 1-form on B defined by

$$(s^*\alpha)_x(v) = \alpha_{s(x)}(s_*v), \quad (104)$$

for any $x \in B$ and $v \in T_x B$, where $s_*: T_x B \rightarrow T_{s(x)} E$ is the pushforward. In spherical coordinates the global connection (26) is written as

$$\mathcal{A} = ig(d\psi + \cos\theta d\phi). \quad (105)$$

The local connection forms (also called gauge potentials) on U_N and U_S are then defined by

$$A_N := f_N^*\mathcal{A}, \quad A_S := f_S^*\mathcal{A}.$$

Using (102)–(105) and the fact that f_N and f_S only change ψ , we obtain

$$A_N = f_N^*\mathcal{A} = ig(d(-\varphi) + \cos\theta d\phi) = -ig(1 - \cos\theta) d\varphi, \quad (106)$$

$$A_S = f_S^*\mathcal{A} = ig(d\varphi + \cos\theta d\phi) = ig(1 + \cos\theta) d\varphi. \quad (107)$$

These 1-forms A_N and A_S are the local connection forms (gauge potentials) on the base S^2 in the northern and southern charts. On the overlap $U_N \cap U_S$ they are related by the gauge transformation.

C.3 Curvature and Chern classes

A crucial notion is then that of **curvature** of a connection. Given two *horizontal* vector fields u, v , their Lie bracket $([u, v](f) := u(v(f)) - v(u(f)))$ is, in general, *not horizontal*: the operator

$$\mathcal{F}(u, v) := \mathcal{A}([u, v]) \quad (108)$$

is the *curvature* of the given connection. Geometrically, $\mathcal{F}(u, v)$ represents the infinitesimal holonomy associated with a small loop spanned by u and v .

The curvature of a connection is defined globally as the 2-form,

$$\mathcal{F} := d\mathcal{A} + \mathcal{A} \wedge \mathcal{A}, \quad (109)$$

where $d\mathcal{A}(u, v) = u(\mathcal{A}(v)) - v(\mathcal{A}(u)) - \mathcal{A}([u, v])$ for *any* vector fields u, v on E and $(\mathcal{A} \wedge \mathcal{A})(u, v) = [\mathcal{A}(u), \mathcal{A}(v)]$. When dealing with the case of a **principal bundle** — wherein $F = G$, a Lie group, called *structure group* freely acting on fibres, namely, without fixed points — and if G is abelian, the second term will actually *drop out*. So in our case $G = U(1)$ and $\mathcal{F} = d\mathcal{A}$. Stokes' theorem then yields (pulling back the relevant forms to the base via a local section s so that, slightly abusively, we may look at \mathcal{F} as a 2-form $F := s^*\mathcal{F}$ thereon):

$$\int_{\mathcal{C}} A = \int_{\mathcal{D}} dA = \int_{\mathcal{D}} F \quad (110)$$

for a loop \mathcal{C} bounding a 2-dimensional domain \mathcal{D} on the base space and where $A = s^*\mathcal{A}$. The holonomy $\text{Hol}_{\mathcal{A}}(\mathcal{C})$ of the connection \mathcal{A} around \mathcal{C} , i.e. the (generalized) Berry phase will then be

$$\text{Hol}_{\mathcal{A}}(\mathcal{C}) = \exp\left(\int_{\mathcal{C}} A\right) = \exp\left(\int_{\mathcal{D}} F\right) \quad (111)$$

In spherical coordinates introduced above for the S^3 , the pullback of the connection 1-form \mathcal{A} along the canonical local sections f_N and f_S yields the following local gauge potentials on S^2 :

$$A_N = f_N^* \mathcal{A} = ig(d(-\varphi) + \cos \theta d\varphi) = -ig(1 - \cos \theta) d\varphi, \quad (112)$$

$$A_S = f_S^* \mathcal{A} = ig(d\varphi + \cos \theta d\varphi) = ig(1 + \cos \theta) d\varphi. \quad (113)$$

Computing $F = dA$ from either local potential gives

$$F_N = dA_N = -ig d(1 - \cos \theta) \wedge d\varphi = -ig \sin \theta d\theta \wedge d\varphi, \quad (114)$$

$$F_S = dA_S = ig d(1 + \cos \theta) \wedge d\varphi = -ig \sin \theta d\theta \wedge d\varphi. \quad (115)$$

Thus $F_N = F_S =: F$ defines a globally well-defined curvature 2-form on S^2 . For a closed curve $\mathcal{C} \subset S^2$ bounding an oriented surface \mathcal{D} , Stokes' theorem yields

$$\oint_{\mathcal{C}} A_{N/S} = \iint_{\mathcal{D}} F. \quad (116)$$

Since $\sin \theta d\theta \wedge d\varphi$ is the area form on the unit sphere, the integral of the curvature over \mathcal{D} equals the solid angle $\Omega(\mathcal{C})$ enclosed by \mathcal{C} :

$$\iint_{\mathcal{D}} F = -ig \Omega(\mathcal{C}). \quad (117)$$

Finally, integrating the curvature over the whole sphere gives $\iint_{S^2} F = -4\pi ig$. The first Chern number therefore reads

$$c_1 = \frac{1}{-2\pi i} \iint_{S^2} F = 2g, \quad (118)$$

which reduces to $c_1 = 1$ upon choosing the standard normalization $g = \frac{1}{2}$.

D SU(2)-actions and parallel transport

We use again $z_1 = x_1 + ix_2$ and $z_2 = x_3 + ix_4$. A vector field is written in the real basis $(\partial_1, \dots, \partial_4)$. Let $U \in SU(2)$ act on every point of \mathbb{C}^2 (z_1, z_2) as follows:

$$\Phi_U : (z_1, z_2)^T \mapsto (z'_1, z'_2)^T = U (z_1, z_2)^T. \quad (119)$$

This induces a real linear map $Q \in SO(4)$ (compare with rotation in quaternion form) on $x = (x_1, x_2, x_3, x_4)^T$:

$$x' = Q x. \quad (120)$$

We want to find a vector field on S^3 that corresponds to an infinitesimal rotation generated by such a unitary matrix. Now consider the example $U = \cos \delta/2 \mathbb{I} + i \sin \delta/2 \sigma_x$. For this case

$$Q_x = \begin{pmatrix} \cos \delta/2 & 0 & 0 & -\sin \delta/2 \\ 0 & \cos \delta/2 & \sin \delta/2 & 0 \\ 0 & -\sin \delta/2 & \cos \delta/2 & 0 \\ \sin \delta/2 & 0 & 0 & \cos \delta/2 \end{pmatrix}. \quad (121)$$

In the general case (9) we introduce the notation

$$c = \cos \delta/2, \quad s = \sin \delta/2, \quad c_2 = \cos(2\beta), \quad s_2 = \sin(2\beta) \quad (122)$$

and get

$$Q(\delta, \beta) = \begin{pmatrix} c & 0 & s s_2 & -s c_2 \\ 0 & c & s c_2 & s s_2 \\ -s s_2 & -s c_2 & c & 0 \\ s c_2 & -s s_2 & 0 & c \end{pmatrix}, \quad (123)$$

and with an additional σ_z rotation $U = \cos \delta/2 \mathbb{I} + i \sin \delta/2 \sigma_z$, which is not realized via the waveplate

$$Q_z = \begin{pmatrix} c & -s & 0 & 0 \\ s & c & 0 & 0 \\ 0 & 0 & c & s \\ 0 & 0 & -s & c \end{pmatrix}. \quad (124)$$

When considering an infinitesimal rotation we should just take the corresponding generator L_Q to get the corresponding vector field as $\dot{x} = L_Q x$, leading to, e.g.

$$L_z = \begin{pmatrix} 0 & -1 & 0 & 0 \\ 1 & 0 & 0 & 0 \\ 0 & 0 & 0 & 1 \\ 0 & 0 & -1 & 0 \end{pmatrix}. \quad (125)$$

with corresponding vector field

$$u_z = -x_2 \partial_1 + x_1 \partial_2 + \mathbf{x}_4 \partial_3 - \mathbf{x}_3 \partial_4. \quad (126)$$

Analogously,

$$u_x = -x_4 \partial_1 + \mathbf{x}_3 \partial_2 - \mathbf{x}_2 \partial_3 + x_1 \partial_4, \quad (127)$$

$$u_y = \mathbf{x}_3 \partial_1 + x_4 \partial_2 - \mathbf{x}_1 \partial_3 - x_2 \partial_4. \quad (128)$$

Note that they differ from horizontal or vertical vector fields (27), (28). For convenience, we highlighted the non-matching terms in bold. So, a unitary 1-parameter subgroup realizes a specific motion on S^3 along the vector fields, given above, which are not horizontal. This means that, in general, a point in S^3 does not move in the way prescribed by the connection form (21), and when we have a closed curve on the Poincaré sphere, realized by a $SU(2)$ rotation, the lifted curve on the S^3 sphere is not horizontal (see, for example, Fig. 3 in [71] as an instance of non-parallel transport). However, for particular lines, where non-coinciding terms for u_x and u_y are zero, we still move along horizontal vector fields! For example, for u_x we want $x_3 = x_2 = 0$, which means that z_1 is purely real and z_2 is purely imaginary. That corresponds to the great circle with $x = 0$ (16). But σ_x corresponds to the rotation of the Poincaré sphere around the x-axis, which means that the motion in S^3 induced by that along a great circle in S^2 is indeed dictated by parallel transport. Similarly, we can consider other rotation angles of the waveplate, however, moving on a great circle of S^2 provides a necessary condition for the phase to be geometric.

E Interpretation in terms of coherent states

The preceding observations could be rephrased via Perelomov's coherent states ([65, 72, 73], see also [69]). In physical terms, let us choose a state on the Poincaré sphere, for instance, a pole. Any transformation, which belongs to the group $SU(2)$ can either move the state to another one, which corresponds to a different point on the sphere, or just introduce some phase (for the pole it would be the subgroup of rotations around the z -axis). In mathematical terms, we consider an action of a compact Lie group G ($SU(2)$ in our case) on a finite-dimensional

vector space V (space of polarization states) and obtain the orbit of this action on a vector $|\xi\rangle \in V$:

$$\{U(g)|\xi\rangle \mid |\xi\rangle \in V\} \cong G/H \quad (129)$$

where H , called the isotropy group of $|\xi\rangle$ (in our case H is $U(1)$ and G/H is topologically S^2), satisfies

$$U(h)|\xi\rangle = e^{i\{\alpha(h)\}}|\xi\rangle \quad (130)$$

with $e^{i\alpha(\cdot)}$ a character of H , namely, a one-dimensional representation of H :

$$e^{i\{\alpha(h_1 h_2)\}} = e^{i\{\alpha(h_1)\}} e^{i\{\alpha(h_2)\}}, \quad h_1, h_2 \in H \quad (131)$$

(necessarily abelian). The above arrangement is termed *coherent state system associated to the representation $U(\cdot)$ and the vector $|\xi\rangle$* . Physically, coherent states are all possible states which can be obtained from a given one by an action of the group. Ultimately, we have a principal bundle with structure group G and base manifold G/H .

A unitary irreducible representation $U(\cdot)$ of $G = SU(2) \cong S^3$ is labelled by its “spin” J and it has dimension $2J + 1$. Here $H = U(1) \cong SO(2) \approx S^1$. Upon taking any vector $|\xi\rangle$ in the ensuing representation space V_J and acting thereon via the representation, we get the coherent state manifold

$$\{U(g)|\xi\rangle \mid |\xi\rangle \in V\} \cong G/H = S^3/S^1 \cong S^2 \quad (132)$$

F Details of numerical simulations

We numerically calculate the phase ϕ of the electric field acquired by rotation of a silicon particle exhibiting different symmetries under illumination by a circularly polarized paraxial Laguerre-Gaussian beam:

$$\mathbf{E}_{\text{in}} \propto (\hat{\mathbf{x}} \pm i\hat{\mathbf{y}})u_{lp}^{\text{LG}}(\mathbf{r}) \quad (133)$$

TAM projection m of such input field can be obtained by writing expression for a circularly polarized field in equivalent form (see Eq. 37):

$$\mathbf{E}_{lp}^{\pm} = e^{\pm i\varphi}(\hat{\boldsymbol{\rho}} \pm i\hat{\boldsymbol{\varphi}})u_{lp}^{LG}(\mathbf{r}) \quad (134)$$

Combining the angular dependencies $e^{\pm i\varphi}e^{il\varphi}$, for the TAM projection of a LG beam we have $m = l \pm 1$. The phase acquired by the rotation of the particle under excitation with a beam ($\lambda = 1550$ nm) having TAM-projection m was determined as follows:

$$\phi_{\pm m} = \arg \left[\int_S \mathbf{E}(\rho, \varphi, z_0) \cdot (\hat{\boldsymbol{\rho}} \mp i\hat{\boldsymbol{\varphi}}) e^{\mp im\varphi} dS \right] \quad (135)$$

where the upper(lower) sign corresponds to the right(left) hand light helicity; the integration was performed over the surface positioned below the particle ($z_0 = -1$ μm). Geometrical parameters of the particles were the following: D_{2h} particle width $w = 263$ nm, height $h = 790$ nm, depth $d = 345$ nm; D_{6h} particle $w = 291$ nm, $h = 700$ nm, the radius of the inscribed circle $R = 922$ nm; D_{3h} particle $w = 591$ nm, $h = 700$ nm, $R = 1300$ nm. Calculations were performed using COMSOL MultiphysicsTM software.

References

- [1] C. Cisowski, J. B. Götte, and S. Franke-Arnold. Colloquium: Geometric phases of light: Insights from fiber bundle theory. *Rev. Mod. Phys.*, 94(3):031001, 2022. ISSN 1539-0756. doi: 10.1103/RevModPhys.94.031001. URL <https://doi.org/10.1103/RevModPhys.94.031001>.
- [2] E. Cohen, H. Larocque, F. Bouchard, F. Nejadsattari, Yu. Gefen, and E. Karimi. Geometric phase from Aharonov–Bohm to Pancharatnam–Berry and beyond. *Nat. Rev. Phys.*, 1(7):437–449, 2019. ISSN 2522-5820. doi: 10.1038/s42254-019-0071-1. URL <https://doi.org/10.1038/s42254-019-0071-1>.
- [3] S. Pancharatnam. Generalized theory of interference, and its applications. *Proc. Indian Acad. Sci.*, 44(5):247–262, 1956. ISSN 0370-0089. doi: 10.1007/BF03046050. URL <https://doi.org/10.1007/BF03046050>.
- [4] M. V. Berry. The Adiabatic Phase and Pancharatnam’s Phase for Polarized Light. *J. Mod. Opt.*, 1987. URL <https://www.tandfonline.com/doi/abs/10.1080/09500348714551321>.
- [5] M. Khorasaninejad, W. T. Chen, R. C. Devlin, J. Oh, A. Y. Zhu, and F. Capasso. Metalenses at visible wavelengths: Diffraction-limited focusing and subwavelength resolution imaging. *Science*, 352(6290):1190–1194, 2016. doi: 10.1126/science.aaf6644. URL <https://www.science.org/doi/abs/10.1126/science.aaf6644>.
- [6] X. Ding, F. Monticone, K. Zhang, L. Zhang, D. Gao, S. N. Burokur, A. de Lustrac, Q. Wu, C.-W. Qiu, and A. Alù. Ultrathin Pancharatnam–Berry Metasurface with Maximal Cross-Polarization Efficiency. *Adv. Mater.*, 27(7):1195–1200, 2015. ISSN 0935-9648. doi: 10.1002/adma.201405047. URL <https://doi.org/10.1002/adma.201405047>.
- [7] W. Luo, S. Sun, H.-X. Xu, Q. He, and L. Zhou. Transmissive Ultrathin Pancharatnam–Berry Metasurfaces with nearly 100% Efficiency. *Phys. Rev. Appl.*, 7(4):044033, 2017. ISSN 2331-7019. doi: 10.1103/PhysRevApplied.7.044033. URL <https://doi.org/10.1103/PhysRevApplied.7.044033>.
- [8] X. Xie, M. Pu, J. Jin, M. Xu, Y. Guo, X. Li, P. Gao, X. Ma, and X. Luo. Generalized Pancharatnam–Berry Phase in Rotationally Symmetric Meta-Atoms. *Phys. Rev. Lett.*, 126(18):183902, 2021. ISSN 1079-7114. doi: 10.1103/PhysRevLett.126.183902. URL <https://doi.org/10.1103/PhysRevLett.126.183902>.
- [9] L. Marrucci, C. Manzo, and D. Paparo. Pancharatnam–Berry phase optical elements for wave front shaping in the visible domain: Switchable helical mode generation. *Appl. Phys. Lett.*, 88(22), 2006. ISSN 0003-6951. doi: 10.1063/1.2207993. URL <https://doi.org/10.1063/1.2207993>.
- [10] L. Huang, X. Chen, H. Mühlenbernd, G. Li, B. Bai, Q. Tan, G. Jin, T. Zentgraf, and S. Zhang. Dispersionless Phase Discontinuities for Controlling Light Propagation. *Nano Lett.*, 12(11):5750–5755, 2012. ISSN 1530-6984. doi: 10.1021/nl303031j. URL <https://doi.org/10.1021/nl303031j>.
- [11] Q. Deng, J. Yang, X. Lan, W. Zhang, H. Cui, Z. Xie, L. Li, and Y. Huang. Investigations of generalized pancharatnam–berry phase in all-dielectric metasurfaces.

Results in Physics, 51:106730, 2023. ISSN 2211-3797. doi: <https://doi.org/10.1016/j.rinp.2023.106730>. URL <https://www.sciencedirect.com/science/article/pii/S2211379723005235>.

[12] D. Wen, F. Yue, G. Li, G. Zheng, K. Chan, S. Chen, M. Chen, K. F. Li, P. W. H. Wong, K. W. Cheah, E. Yue Bun Pun, S. Zhang, and X. Chen. Helicity multiplexed broadband metasurface holograms. *Nature Communications*, 6:8241, 2015. doi: 10.1038/ncomms9241. URL <https://doi.org/10.1038/ncomms9241>.

[13] G. Zheng, H. Mühlenbernd, M. Kenney, G. Li, T. Zentgraf, and S. Zhang. Metasurface holograms reaching 80% efficiency. *Nature Nanotechnology*, 10(4):308–312, 2015. doi: 10.1038/nnano.2015.2. URL <https://www.nature.com/articles/nnano.2015.2>.

[14] E. J. Galvez, P. R. Crawford, H. I. Sztul, M. J. Pysher, P. J. Haglin, and R. E. Williams. Geometric Phase Associated with Mode Transformations of Optical Beams Bearing Orbital Angular Momentum. *Phys. Rev. Lett.*, 90(20):203901, 2003. ISSN 1079-7114. doi: 10.1103/PhysRevLett.90.203901. URL <https://doi.org/10.1103/PhysRevLett.90.203901>.

[15] M. J. Padgett and J. Courtial. Poincaré-sphere equivalent for light beams containing orbital angular momentum. *Opt. Lett.*, 24(7):430–432, 1999. ISSN 0146-9592. doi: 10.1364/ol.24.000430. URL <https://doi.org/10.1364/ol.24.000430>.

[16] S. J. van Enk. Geometric phase, transformations of gaussian light beams and angular momentum transfer. *Opt. Commun.*, 102(1):59–64, 1993. ISSN 0030-4018. doi: 10.1016/0030-4018(93)90472-H. URL [https://doi.org/10.1016/0030-4018\(93\)90472-H](https://doi.org/10.1016/0030-4018(93)90472-H).

[17] S. J. M. Habraken and G. Nienhuis. Universal description of geometric phases in higher-order optical modes bearing orbital angular momentum. *Opt. Lett.*, 35(20):3535–3537, 2010. ISSN 1539-4794. doi: 10.1364/OL.35.003535. URL <https://doi.org/10.1364/OL.35.003535>.

[18] S. J. M. Habraken and G. Nienhuis. Geometric phases in higher-order transverse optical modes. In *Proceedings Volume 7613, Complex Light and Optical Forces IV*, volume 7613, pages 121–128. SPIE, 2010. doi: 10.1117/12.840024. URL <https://doi.org/10.1117/12.840024>.

[19] B. Simon. Holonomy, the Quantum Adiabatic Theorem, and Berry’s Phase. *Phys. Rev. Lett.*, 51(24):2167–2170, 1983. ISSN 1079-7114. doi: 10.1103/PhysRevLett.51.2167. URL <https://doi.org/10.1103/PhysRevLett.51.2167>.

[20] H. Takenaka. A unified formalism for polarization optics by using group theory. *Nouv. Rev. Opt.*, 4(1):37, January 1973. ISSN 0335-7368. doi: 10.1088/0335-7368/4/1/304. URL <https://doi.org/10.1088/0335-7368/4/1/304>.

[21] D. Susic, R. Droop, E. Otte, D. Ehrmanntraut, F. Nori, J. Ruostekoski, C. Denz, and M. R. Dennis. Particle-like topologies in light. *Nat. Commun.*, 12(6785):1–10, 2021. ISSN 2041-1723. doi: 10.1038/s41467-021-26171-5. URL <https://doi.org/10.1038/s41467-021-26171-5>.

[22] B. Jurčo. Polarization of light and hopf fibration. *Czech. J. Phys.*, 37(9):1035–1038, September 1987. ISSN 1572-9486. doi: 10.1007/BF01597447. URL <https://doi.org/10.1007/BF01597447>.

[23] Vektorfeld. From Poincaré sphere (Bloch sphere) to Projective space, November 2025. URL <https://www.youtube.com/watch?v=Qun3gahLP3o>.

[24] S. Gladyshev, K. Frizyuk, and A. Bogdanov. Symmetry analysis and multipole classification of eigenmodes in electromagnetic resonators for engineering their optical properties. *Phys. Rev. B*, 102(7):075103, 2020. ISSN 2469-9969. doi: 10.1103/PhysRevB.102.075103. URL <https://doi.org/10.1103/PhysRevB.102.075103>.

[25] Z. Xiong, Q. Yang, W. Chen, Z. Wang, J. Xu, W. Liu, and Y. Chen. On the constraints of electromagnetic multipoles for symmetric scatterers: eigenmode analysis. *Opt. Express*, 28(3):3073–3085, 2020. ISSN 1094-4087. doi: 10.1364/OE.382239. URL <https://doi.org/10.1364/OE.382239>.

[26] A. A. Shumitskaya, V. O. Kozlov, N. I. Selivanov, C. C. Stoumpos, V. S. Zapasskii, Yu. V. Kapitonov, and I. I. Ryzhov. The Faraday Effect and Phase Transition in the CH₃NH₃PbI₃ Halide Perovskite Single Crystal. *Adv. Opt. Mater.*, 12(10):2302095, April 2024. ISSN 2195-1071. doi: 10.1002/adom.202302095. URL <https://doi.org/10.1002/adom.202302095>.

[27] J. C. Garrison and R. Y. Chiao. Geometrical Phases from Global Gauge Invariance of Nonlinear Classical Field Theories. *Phys. Rev. Lett.*, 60(3):165–168, January 1988. doi: 10.1103/PhysRevLett.60.165. URL <https://doi.org/10.1103/PhysRevLett.60.165>.

[28] A. Zee. *Group Theory in a Nutshell for Physicists*. Princeton University Press, Princeton, NJ, USA, 2016. ISBN 978-0-69116269-0. URL <https://www.amazon.com/Group-Theory-Nutshell-Physicists-Zee/dp/0691162697>.

[29] S. Saito. Quantum field theory for coherent photons: isomorphism between Stokes parameters and spin expectation values. *Front. Phys.*, 11:1225334, 2024. ISSN 2296-424X. doi: 10.3389/fphy.2023.1225334. URL <https://doi.org/10.3389/fphy.2023.1225334>.

[30] S. Saito. SU(2) symmetry of coherent photons and application to Poincaré rotator. *Front. Phys.*, 11:1225419, July 2023. ISSN 2296-424X. doi: 10.3389/fphy.2023.1225419. URL <https://doi.org/10.3389/fphy.2023.1225419>.

[31] Quantum Mechanic (<https://physics.stackexchange.com/users/291677/quantum-mechanic>). What are the stokes parameters of a linear wave added to a circular one? Physics Stack Exchange, 2021. URL <https://physics.stackexchange.com/q/638919>.

[32] G. F. Torres del Castillo and I. Rubalcava-Garcia. The Jones vector as a spinor and its representation on the Poincaré sphere. *arXiv*, March 2013. doi: 10.48550/arXiv.1303.4496. URL <https://doi.org/10.48550/arXiv.1303.4496>.

[33] F. P. Schuller. Lectures on the geometric anatomy of theoretical physics. *Institute for Quantum Gravity*, Friedrich-Alexander Universität Erlangen-Nürnberg, 2015.

[34] D. Chruściński and A. Jamiołkowski. *Geometric Phases in Classical and Quantum Mechanics*. Birkhäuser, Boston, MA, USA, 2004. ISBN 978-0-8176-8176-0. URL <https://link.springer.com/book/10.1007/978-0-8176-8176-0>.

[35] M. Nakahara. *Geometry, Topology and Physics, Second Edition (Graduate Student Series in Physics)*. CRC Press, Boca Raton, FL, USA, 2003. ISBN 978-0-75030606-5.

[36] J. Anandan and L. Stodolsky. Some geometrical considerations of Berry's phase. *Phys. Rev. D*, 35(8):2597–2600, 1987. ISSN 2470-0029. doi: 10.1103/PhysRevD.35.2597. URL <https://doi.org/10.1103/PhysRevD.35.2597>.

[37] J. Anandan. The geometric phase. *Nature*, 360(6402):307–313, 1992. ISSN 1476-4687. doi: 10.1038/360307a0. URL <https://doi.org/10.1038/360307a0>.

[38] N. Johnson. Hopf fibration – fibers and base, August 2011. URL <https://www.youtube.com/watch?v=AKotMPGFJYk>.

[39] H. Urbantke. Two-level quantum systems: States, phases, and holonomy. *Am. J. Phys.*, 59(6):503–509, 1991. ISSN 0002-9505. doi: 10.1119/1.16809. URL <https://doi.org/10.1119/1.16809>.

[40] A. A. Voitiv, M. T. Lusk, and M. E. Siemens. Experimental measurement of the geometric phase of non-geodesic circles. *Opt. Lett.*, 48(10):2680–2683, 2023. ISSN 1539-4794. doi: 10.1364/OL.489899. URL <https://doi.org/10.1364/OL.489899>.

[41] N. Hagen and L. Garza-Soto. Evolution of geometric phase and explaining the geodesic rule. *J. Opt. Soc. Am. A*, 41(11):2014–2022, Nov 2024. doi: 10.1364/JOSAA.538106. URL <https://doi.org/10.1364/JOSAA.538106>.

[42] Y. Shen. Rays, waves, SU(2) symmetry and geometry: toolkits for structured light. *J. Opt.*, 23(12):124004, 2021. ISSN 2040-8986. doi: 10.1088/2040-8986/ac3676. URL <https://doi.org/10.1088/2040-8986/ac3676>.

[43] A. Nikitina and K. Frizyuk. Achiral Nanostructures: Perturbative Harmonic Generation and Dichroism Under Vortex and Vector Beams Illumination. *Adv. Opt. Mater.*, n/a (n/a):2400732, 2024. ISSN 2195-1071. doi: 10.1002/adom.202400732. URL <https://doi.org/10.1002/adom.202400732>.

[44] Q. Zhan. Properties of circularly polarized vortex beams. *Opt. Lett.*, 31(7):867–869, 2006. ISSN 1539-4794. doi: 10.1364/OL.31.000867. URL <https://doi.org/10.1364/OL.31.000867>.

[45] E. Hasman, V. Kleiner, G. Biener, and A. Niv. Polarization dependent focusing lens by use of quantized Pancharatnam–Berry phase diffractive optics. *Appl. Phys. Lett.*, 82(3): 328–330, 2003. ISSN 0003-6951. doi: 10.1063/1.1539300. URL <https://doi.org/10.1063/1.1539300>.

[46] Q. Song, A. Baroni, R. Sawant, P. Ni, V. Brandli, S. Chenot, S. Vézian, B. Damilano, P. de Mierry, S. Khadir, P. Ferrand, and P. Genevet. Ptychography retrieval of fully polarized holograms from geometric-phase metasurfaces. *Nat. Commun.*, 11(2651):1–8, 2020. ISSN 2041-1723. doi: 10.1038/s41467-020-16437-9. URL <https://doi.org/10.1038/s41467-020-16437-9>.

[47] Adam C. Overvig, Sajan Shrestha, Stephanie C. Malek, Ming Lu, Aaron Stein, Changxi Zheng, and Nanfang Yu. Dielectric metasurfaces for complete and independent control of the optical amplitude and phase. *Light Sci. Appl.*, 8(92):1–12, 2019. ISSN 2047-7538. doi: 10.1038/s41377-019-0201-7. URL <https://doi.org/10.1038/s41377-019-0201-7>.

[48] G. Guercio, A. Gerini, K. Frizyuk, C. De Angelis, M. Morassi, A. Lemaître, L. Carletti, and G. Leo. Tensor-driven geometric phase in nonlinear algaas metasurfaces, 2026. URL <https://arxiv.org/abs/2601.18246>.

[49] M. Lax, W. H. Louisell, and W. B. McKnight. From Maxwell to paraxial wave optics. *Phys. Rev. A*, 11(4):1365–1370, 1975. ISSN 2469-9934. doi: 10.1103/PhysRevA.11.1365. URL <https://doi.org/10.1103/PhysRevA.11.1365>.

[50] G. Nienhuis and L. Allen. Paraxial wave optics and harmonic oscillators. *Phys. Rev. A*, 48(1):656–665, 1993. ISSN 2469-9934. doi: 10.1103/PhysRevA.48.656. URL <https://doi.org/10.1103/PhysRevA.48.656>.

[51] H. Kogelnik and T. Li. Laser Beams and Resonators. *Appl. Opt.*, 5(10):1550–1567, 1966. ISSN 2155-3165. doi: 10.1364/AO.5.001550. URL <https://doi.org/10.1364/AO.5.001550>.

[52] G. Nienhuis and J. Visser. Angular momentum and vortices in paraxial beams. *J. Opt. A: Pure Appl. Opt.*, 6(5):S248, 2004. ISSN 1464-4258. doi: 10.1088/1464-4258/6/5/020. URL <https://doi.org/10.1088/1464-4258/6/5/020>.

[53] M. W. Beijersbergen, L. Allen, H. E. L. O. van der Veen, and J. P. Woerdman. Astigmatic laser mode converters and transfer of orbital angular momentum. *Opt. Commun.*, 96(1): 123–132, 1993. ISSN 0030-4018. doi: 10.1016/0030-4018(93)90535-D. URL [https://doi.org/10.1016/0030-4018\(93\)90535-D](https://doi.org/10.1016/0030-4018(93)90535-D).

[54] M. R. Dennis and M. A. Alonso. Swings and roundabouts: optical Poincaré spheres for polarization and Gaussian beams. *Philos. Trans. Royal Soc. A*, 375(2087), 2017. ISSN 1471-2962. doi: 10.1098/rsta.2015.0441. URL <https://doi.org/10.1098/rsta.2015.0441>.

[55] G. F. Calvo. Wigner representation and geometric transformations of optical orbital angular momentum spatial modes. *Opt. Lett.*, 30(10):1207–1209, 2005. ISSN 1539-4794. doi: 10.1364/OL.30.001207. URL <https://doi.org/10.1364/OL.30.001207>.

[56] R. Simon and G. S. Agarwal. Wigner representation of Laguerre–Gaussian beams. *Opt. Lett.*, 25(18):1313–1315, 2000. ISSN 1539-4794. doi: 10.1364/OL.25.001313. URL <https://doi.org/10.1364/OL.25.001313>.

[57] L. Allen, J. Courtial, and M. J. Padgett. Matrix formulation for the propagation of light beams with orbital and spin angular momenta. *Phys. Rev. E*, 60(6):7497–7503, 1999. ISSN 2470-0053. doi: 10.1103/PhysRevE.60.7497. URL <https://doi.org/10.1103/PhysRevE.60.7497>.

[58] P. Albers, H. Geiges, and K. Zehmisch. A Symplectic Dynamics Proof of the Degree–Genus Formula. *Arnold Math. J.*, 9(1):41–68, 2023. ISSN 2199-6806. doi: 10.1007/s40598-021-00195-7. URL <https://doi.org/10.1007/s40598-021-00195-7>.

[59] Randy S. The Hopf Bundle: an Example of a Nontrivial Principal Bundle . *cphysics.org*, 2024. URL <https://www.cphysics.org/article/03838.pdf>.

[60] U. Bruzzo, P. Fré, U. Shahzad, and M. Trigiante. D3-brane supergravity solutions from Ricci-flat metrics on canonical bundles of Kähler–Einstein surfaces. *Lett. Math. Phys.*, 113(3):64–70, 2023. ISSN 1573-0530. doi: 10.1007/s11005-023-01683-x. URL <https://doi.org/10.1007/s11005-023-01683-x>.

[61] C. H. Lee and C. H. Tan. Topology and Geometry of 3-Band Models. In *IRC-SET 2021*, pages 59–81. Springer, Singapore, 2022. ISBN 978-981-16-9869-9. doi: 10.1007/978-981-16-9869-9_5. URL https://doi.org/10.1007/978-981-16-9869-9_5.

[62] Julian Schwinger. *On Angular Momentum* (Dover Books on Physics). Dover Publications, Mineola, NY, USA, 2015. ISBN 978-0-48678810-4. URL <https://www.amazon.com/Angular-Momentum-Dover-Books-Physics/dp/0486788105>.

[63] S. Shabbir. Majorana Representation in Quantum Optics : SU(2) Interferometry and Uncertainty Relations. PhD thesis, KTH Royal Institute of Technology, 2017. URL <http://www.diva-portal.org/smash/record.jsf?pid=diva2%3A1091994&dswid=-7801>.

[64] E. Majorana. Atomi orientati in campo magnetico variabile. *Nuovo Cim.*, 9(2):43–50, 1932. ISSN 1827-6121. doi: 10.1007/BF02960953. URL <https://doi.org/10.1007/BF02960953>.

[65] R. Gutiérrez-Cuevas, S. A. Wadood, A. N. Vamivakas, and M. A. Alonso. Modal Majorana Sphere and Hidden Symmetries of Structured-Gaussian Beams. *Phys. Rev. Lett.*, 125(12):123903, 2020. ISSN 1079-7114. doi: 10.1103/PhysRevLett.125.123903. URL <https://doi.org/10.1103/PhysRevLett.125.123903>.

[66] M. Tymchenko, J. S. Gomez-Diaz, J. Lee, N. Nookala, M. A. Belkin, and A. Alù. Gradient nonlinear pancharatnam-berry metasurfaces. *Phys. Rev. Lett.*, 115:207403, Nov 2015. doi: 10.1103/PhysRevLett.115.207403. URL <https://link.aps.org/doi/10.1103/PhysRevLett.115.207403>.

[67] N. Sansonetto and M. Spera. Hamiltonian monodromy via geometric quantization and theta functions. *Journal of Geometry and Physics*, 60(3):501–512, 2010. ISSN 0393-0440. doi: <https://doi.org/10.1016/j.geomphys.2009.11.012>. URL <https://doi.org/10.1016/j.geomphys.2009.11.012>.

[68] V. Penna and M. Spera. Remarks on quantum vortex theory on riemann surfaces. *Journal of Geometry and Physics*, 27(1):99–112, 1998. ISSN 0393-0440. doi: [https://doi.org/10.1016/S0393-0440\(97\)00070-3](https://doi.org/10.1016/S0393-0440(97)00070-3). URL [https://doi.org/10.1016/S0393-0440\(97\)00070-3](https://doi.org/10.1016/S0393-0440(97)00070-3).

[69] G. Barbieri, K. Frizyuk, and M. Spera. On the geometry and braiding of optical phases. Available at SSRN 5371800, 2025.

[70] K. Y. Bliokh, M. A. Alonso, and M. R Dennis. Geometric phases in 2d and 3d polarized fields: geometrical, dynamical, and topological aspects. *Reports on Progress in Physics*, 82(12):122401, oct 2019. doi: 10.1088/1361-6633/ab4415. URL <https://doi.org/10.1088/1361-6633/ab4415>.

[71] J. Courtial. Wave plates and the Pancharatnam phase. *Opt. Commun.*, 171(4):179–183, December 1999. ISSN 0030-4018. doi: 10.1016/S0030-4018(99)00473-3. URL [https://doi.org/10.1016/S0030-4018\(99\)00473-3](https://doi.org/10.1016/S0030-4018(99)00473-3).

[72] A. Perelomov. *Generalized Coherent States and Their Applications*. Springer, Berlin, Germany, 1986. ISBN 978-3-642-61629-7. URL <https://link.springer.com/book/10.1007/978-3-642-61629-7>.

[73] H. Kuratsuji. Geometric phase accompanying SU(2) coherent states for quantum polarized light. *Phys. Rev. A*, 88(3):033801, September 2013. doi: 10.1103/PhysRevA.88.033801. URL <https://doi.org/10.1103/PhysRevA.88.033801>.